# In Situ Biomineralization of $Cu_xZn_ySn_zS_4$ Nanocrystals within TiO_2-Based Quantum Dot Sensitized Solar Cell Anodes

Abdolhamid Sadeghnejad,[†] Li Lu,[‡] Joseph Cline,[‡] Nur K. Ozdemir,[†] Mark A. Snyder,[†] Christopher J. Kiely,[†,‡] and Steven McIntosh*,[†]

[†]Department of Chemical and Biomolecular Engineering and [‡]Department of Materials Science and Engineering, Lehigh University, Bethlehem, Pennsylvania 18015, United States

S *Supporting Information*
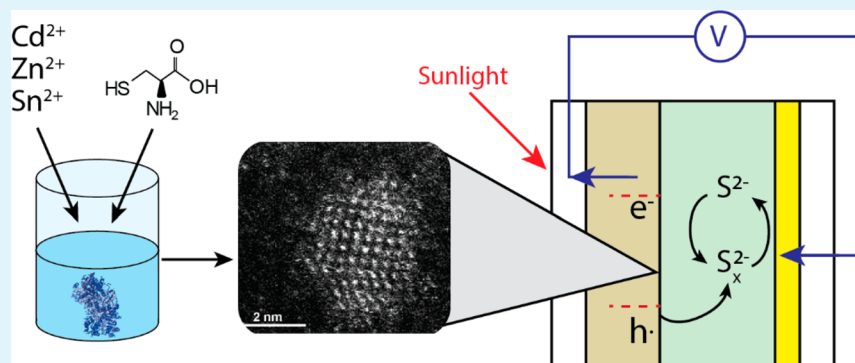
ABSTRACT: CuZnSnS (CZTS) quantum dots (QDs) have potential application in quantum dot sensitized solar cells (QDSSCs); however, traditional synthesis approaches typically require elevated temperatures, expensive precursors, and organic solvents that can hinder large-scale application. Herein we develop and utilize an enzymatic, aqueous-phase, ambient temperature route to prepare CZTS nanocrystals with good compositional control. Nanoparticle synthesis occurs in a minimal buffered solution containing only the enzyme, metal chloride and acetate salts, and L-cysteine as a capping agent and sulfur source. Beyond isolated nanocrystal synthesis, we further demonstrate biomineralization of these particles within a preformed mesoporous TiO_2 anode template where the formed nanocrystals bind to the TiO_2 surface. This in situ biomineralization approach facilitates enhanced distribution of the nanocrystals in the anode and, through this, enhanced QDSSC performance.

KEYWORDS: quantum dots, biomineralization, quantum dot sensitized solar cells (QDSSC), nanocrystals, copper zinc tin sulfide, nanocrystals, green synthesis

1. INTRODUCTION

Quantum confined metal chalcogenide nanocrystals find potential application as sensitizers in quantum dot sensitized solar cells (QDSSCs) due to their size-tunable optical band gap, high extinction coefficient, potential stability, and ease of fabrication when compared with molecular dyes.[1−3] As with any potential large-scale energy technology, a challenge in scaling up production of these devices to impactful levels will lie in minimizing the environmental impact and energy demands of nanocrystal synthesis. Typical nanocrystal synthesis routes utilize elevated temperatures, organic solvents, and expensive precursors that, while providing high performance nanomaterials, present challenges in meeting these environmental impact goals. Beyond these synthesis demands, the use of nontoxic, earth abundant materials as the QDs themselves will likely be critical in promoting wider application.

One class of materials of particular interest is the kesterite family of $Cu_xZn_ySn_zS(Se)_4$ (CZTS) compounds,[4−6] as they are direct band gap semiconductor materials with tunable band gap in the desirable 1.0−1.5 eV range.[4] These materials have been extensively researched for incorporation into photovoltaic devices, most commonly as thin films[7] and as sensitizers on TiO_2-based anodes.[8−11] The performance in photovoltaic devices is reported to depend on the cation ratios within CZTS, with target compositions suggested as Cu/Zn + Sn and Zn/Sn in CZTS in the ranges of 0.73−0.96 and 1.00−1.71, respectively, with the stoichiometric Cu_2ZnSnS_4 typically utilized in the highest performance electrodes.

However, even with these more benign materials, there is a persistent challenge to develop benign processes for nanocrystal synthesis and formation of films from these nanocrystal inks. Typical CZTS nanocrystal synthesis is conducted via pyrolysis, where organometallic precursors are rapidly injected into a hot organic solution to facilitate rapid particle formation and control size.[6,12−16] While the resulting particle composition reflects the ratio of injected metal cations, Cu deficiency[6]

and Sn enrichment[16] relative to Cu_2ZnSnS_4 are both frequently reported[17] and have been suggested to lead to improved performance.[17,18] Some of the highest efficiency photovoltaic cells have utilized thin CZTS films formed by the deposition of small nanocrystals followed by thermal annealing.[17,19] These processes typically utilize organic solvents, vacuum processing, and elevated temperature annealing. Perhaps the highest efficiency has been achieved using hydrazine as a solvent,[20,21] which is highly undesirable at industrial scale. A number of more benign approaches have been suggested.[22] One frequently pursued alternative that enables the use of benign and even aqueous solvents is successive ionic layer adsorption and reaction (SILAR), which utilizes multistep deposition, followed by a high temperature anneal to synthesize a CZTS film.[20,23−28]

Our group has recently developed an alternative bioinspired enzymatic biomineralization route to the ambient temperature, aqueous-phase, size-controlled synthesis of metal sulfide and metal selenide quantum confined nanocrystals as single compositions, alloys, and core−shell heterostructures. This is achieved by utilizing an engineered cystathionine γ-lyase enzyme that actively turns over the amino acid L-cysteine in solution to form reactive sulfur, likely HS^-. This sulfur can then react with a metal ion in solution to form a metal sulfide. Through careful tuning of the growth conditions, solution composition, and relative enzyme activity, high quality, size-controlled nanocrystals can be formed in a minimal buffered aqueous solution containing the metal salt, enzyme, and L-cysteine as the sulfur source and capping agent.[29,30] While these quantum dots have numerous potential applications, the benign synthesis of environmentally benign CZTS sensitizers for QDSSCs is an attractive proposition.

Incorporation of QD sensitizers into the TiO_2 layer of the QDSSC anode is commonly achieved through chemical bath deposition where nucleation and growth of the QDs occurs directly on an immersed TiO_2 substrate.[31,32] Alternative approaches include SILAR-based methods and the incorporation of externally synthesized QDs either by physisorption or using tether molecules. In all cases, it is desirable to obtain a uniform distribution of the sensitizer within the mesoporous TiO_2 layer to achieve a high active surface area. We have previously reported an unoptimized QDSSC where biomineralized PbS and PbS@CdS core@shell nanocrystals were added to a mesoporous TiO_2 layer by a simple drop-casting approach.[33]

In the current work, we address two challenges around this goal, namely the synthesis of a ternary metal sulfide in the CZTS family with control of composition within the most active target range and the efficient integration and dispersion of these materials into a TiO_2 electrode mesostructured through in situ biomineralization of the CZTS nanocrystals within the preformed TiO_2 structure.

2. EXPERIMENTAL SECTION

2.1. Enzyme Expression and Purification. Biomineralization of quantum confined metal sulfide nanocrystals via the smCSE enzyme has been described in detail in previous publications.[30,34−36] Briefly, the expression of smSCE cloned within a BL21 strain of E. coli was started by subculturing the plasmid in 200 mL of LB broth at 37 °C for 16 h. The main expression was induced at dilution of OD_{600} = 0.8 by adding an additional 800 mL of LB broth and 1 mM IPTG at 20 °C and incubating for 16 h. The solution was then centrifuged at 3225g for 10 min, and the pellet was resuspended in lysis buffer and sonicated for 30 min. The sonicated solution was centrifuged at 3225g for 10 min prior to enzyme purification via immobilized metal affinity chromatography[38] with 500 mM imidazole buffer. The purified enzyme was stored at 4 °C prior to use in further experiments.

2.2. SnS and CZTS Biomineralization. SnS nanocrystal synthesis was achieved through incubation of a buffered solution (Tris−HCl at pH 7) of tin(II) chloride (Alfa Aesar, anhydrous, 98%), L-cysteine (8.25 mM, Spectrum Chemicals, 99.55%), and purified smCSE enzyme (OD_{600} = 500) incubated at 37 °C for 6 h. As with our previous reports, particle formation occurs by reaction of the metal cations with reactive sulfur formed by the enzymatic turnover of L-cysteine by smCSE. An identical procedure was utilized for the biomineralization of $Cu_xZn_ySn_zS_4$ (CZTS) alloy nanoparticles by replacing tin(II) chloride with a mixtures of tin(II) chloride, copper acetate (Alfa Aesar Puratronic, 99.995% metals basis), and zinc acetate (Alfa Aesar Puratronic, 99.995% metals basis). Optimization of the CZTS composition within the biomineralized nanocrystals was pursued by changing the molar ratio of Cu:Zn:Sn in the synthesis solution. After synthesis, the nanoparticles were precipitated with ethanol as well as centrifuged at 3225g for 15 min, and the resulting pellet was resuspended in deionized water.

2.3. Material Characterization. Ultraviolet−visible (UV−vis) absorbance spectra (2600 Shimadzu spectrophotometer with an ISR-2600-Plus integrating sphere) and corresponding photoluminescence spectra (QuantaMaster 400 spectrometer) of the biosynthesized nanocrystals were recorded at periodic intervals during synthesis and after synthesis.

TEM samples were prepared by dialyzing the solution containing the nanocrystals against deionized water. The solution was then diluted and drop-cast onto a holey carbon film supported on a Ni-mesh grid. High angle annular dark field (HAADF) and bright field (BF) scanning transmission electron microscopy (STEM) imaging and X-ray energy-dispersive spectroscopy (XEDS) experiments were conducted at 200 kV using an aberration corrected JEOL ARM 200CF analytical electron microscope equipped with a JEOL Centurio XEDS system. Digital Micrograph and JEMS software were used to filter and analyze the STEM images, while ImageJ was used to quantify particle size distributions. DTSA-II software was used to model the XEDS results. Additional scanning electron microscopy (SEM) images and XEDS spectra were obtained from centrifuged and dried nanocrystal samples and completed solar cells using a Hitachi 4300SE/N FEG-SEM operating at 20 kV, which was equipped with an EDAX-SDD energy-dispersive X-ray spectrometer.

2.4. QDSSC Fabrication and Testing. Two approaches were adopted to prepare quantum dot sensitized TiO_2 solar cell anodes, namely, (i) drop-casting of preformed QDs onto a TiO_2 matrix and (ii) in situ growth of QDs within the TiO_2 matrix. The TiO_2 anode structure was formed utilizing a standard process. FTO glass (Sigma-Aldrich, 7 Ω sq^{-1}) was cleaned by sonication in a Contrad 70 soap and deionized water solution for 15 min, followed by sonication in ethanol for 15 min.[36] The TiO_2 layer was formed utilizing the approach previously reported by Kumnorkaew et al.[37] A TiO_2 blocking layer (13 μm thick) was deposited on the clean FTO by submerging the glass at 70 °C for 30 min in diluted $TiCl_4$ (40 mM) solution. A 1 cm^2 area of the dried and washed substrates was coated with TiO_2 paste (opaque titania paste, Sigma-Aldrich) utilizing a doctor blade and Scotch magic tape (3M) to set the height. Annealing the resulting structure at 450 °C for 1.5 h led to a 13 μm thick porous coating of TiO_2 on the FTO substrate. Drop-cast electrodes were prepared by depositing 20 μL of as-synthesized biomineralized QD solution onto the anode with overnight drying at room temperature. In situ growth of quantum dots in the anode structure was achieved by placing the TiO_2-coated FTO glass into the biomineralization solutions at the beginning of nanocrystal synthesis and incubating at 37 °C for 6 h. The adsorption of CZTS QDS onto TiO_2 was investigated by mixing as-synthesized CZTS QDs with TiO_2 particles. The mixture was shaken and centrifuged at 3225g for 10 min, and the UV−vis absorbance spectra were measured.

The CuS cathode was prepared by electrochemical deposition of Cu onto cleaned FTO glass followed by sulfidation.[40] The FTO glass was immersed in 9 mM Cu_2SO_4 electrolyte solution with a Cu foil counter electrode, and a current of 80 mA/cm^2 was applied for 2000 cycles containing two steps with −2.0 V for 0.2 s and 0 V for 0.4 s.[38] The deposited Cu was washed with deionized water and
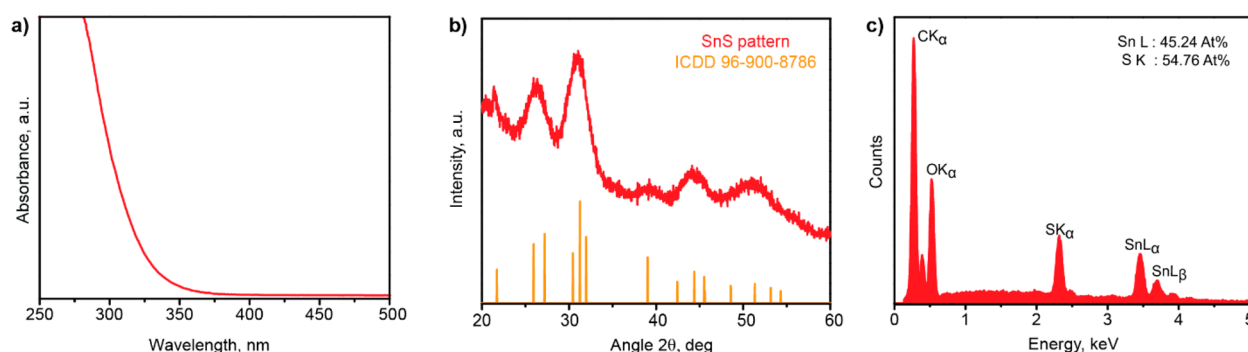
Figure 1. (a) UV−vis absorption spectrum, (b) XRD pattern, and (c) typical SEM−XEDS spectrum acquired from our SnS nanocrystals.

ethanol and dried at room temperature. The Cu-coated FTO was then immersed in 1 M Na_2S solution for 1 min followed by washing with ethanol.[40]

The solar cells were assembled by clamping the two electrodes together with one layer of Parafilm (13 μm) as a spacer and seal. The polysulfide electrolyte, 1 M Na_2S (Alfa Aesar), 1 M S (Alfa Aesar, 99.5%), and 0.1 M NaOH(BDH),[41] was injected into the interstitial space to complete the cell. Electrical connections were made using conductive copper tape (VWR). The electrochemical performance of the cells was analyzed utilizing a Reference 3000 potentiostat (Gamry Instruments). Current density−voltage (J−V) curves were recorded at a linear sweep voltammetry rate of 100 mV/s under 1 sun illumination (Solar Simulator, ABET Technologies). Multiple solar cells were fabricated and tested in at minimum triplicate with average and ranges of J−V performance reported herein.

3. RESULTS AND DISCUSSION

3.1. Biomineralization of CZTS Alloy Nanocrystals.
While we have previously demonstrated the enzymatic biomineralization of Cu and Zn sulfides, the first step in extending this work to CZTS was to confirm biomineralization of tin sulfide nanocrystals. The UV−vis absorption spectra and corresponding photoluminescence spectra resulting from solutions of tin(II) chloride, L-cysteine, and the smCSE enzyme that had been incubated for 6 h are shown in Figure 1a. The absorption feature beginning at 350 nm is consistent with the formation of quantum confined SnS nanocrystals.[39] The corresponding direct optical band gap of 3.3 eV determined from a Tauc plot of the absorption data, Figure S1, is higher than the bulk SnS direct band gap, which is reported to be between 1.30 and 1.43 eV,[40] and is in the range of previous reports for quantum confined SnS nanocrystals.[39]

The X-ray diffraction pattern of the precipitated, centrifuged, and dried particles, Figure 1b, shows broad peaks at positions expected for the orthorhombic structure of SnS. The expected peak positions for SnS having the orthorhombic space group *Pnma* (ICDD 96-900-8786) are shown for reference. The XRD pattern shows peak broadening, consistent with the formation of small nanocrystals, with no observable impurity peaks. SEM−XEDS analysis of the material, Figure 1c, confirms the presence of both Sn and S in the particles. *Note that while it is feasible that some residual chlorine from the synthesis process may be present in the particles, if present, the quantity is below the detection limit of the XEDS instrument when we analyze the as-synthesized particle.*

Direct evidence for the biomineralization of quantum confined SnS nanoparticles is provided by HAADF-STEM imaging and associated XEDS analysis. Figure 2a shows an HAADF-STEM image of a cluster of nanocrystals displaying clear lattice fringes. Analysis of 80 particles yields an average
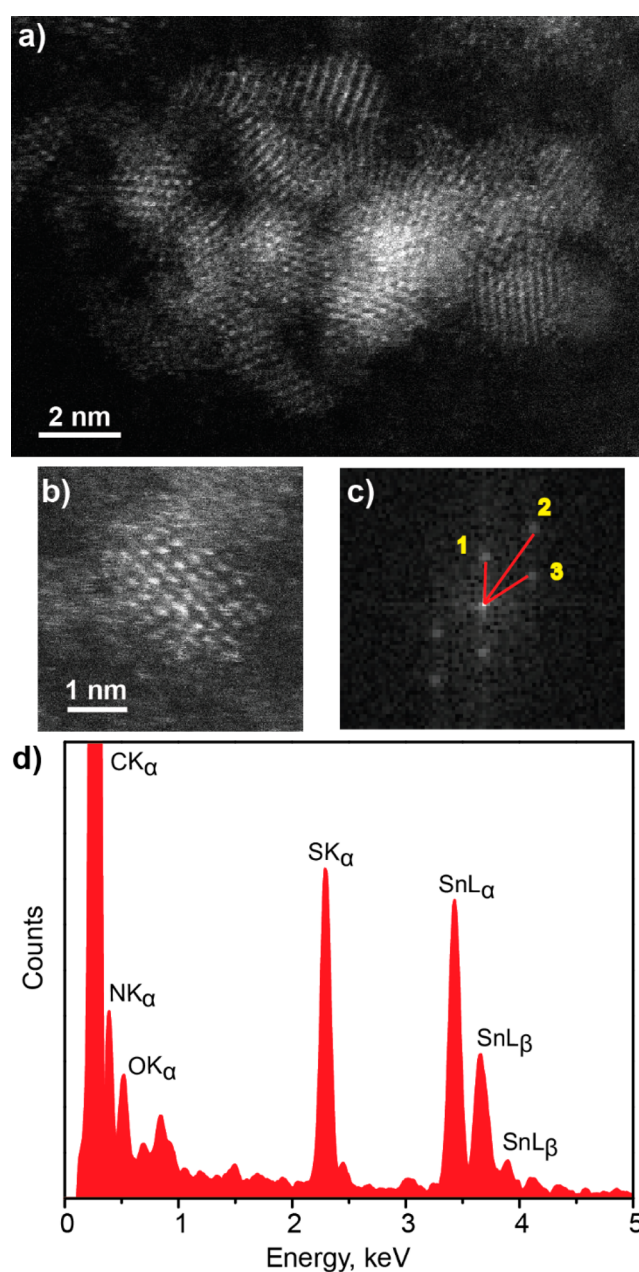
Figure 2. (a,b) Representative HAADF-STEM images, (c) FFT pattern corresponding to the image in b, and (d) STEM−XEDS spectrum of biomineralized SnS showing the coexistence of Sn and S within the nanocrystals.
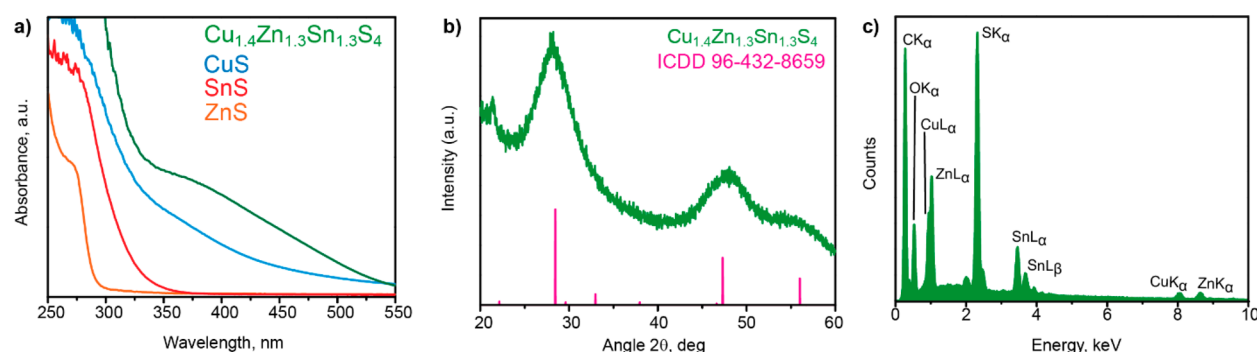
Figure 3. (a) UV−vis absorption of biomineralized crystals formed from solutions with Zn acetate, Cu acetate, Sn chloride, and a mixture ratio of Cu:Zn:Sn = 1:2:2, (b) XRD pattern, and (c) SEM−XEDS spectrum of the synthesized particles.

particle size of 2.25 ± 0.54 nm, Figure S2, which is substantially below the 7 nm Bohr radius reported for SnS.[41,42] Analysis of the lattice fringes of one particle, Figure 2b, by fast-Fourier transform (FFT), Figure 2c, indicates interplanar spacing and angles consistent with orthorhombic SnS viewed along the [001] axis, Table S1. XEDS analysis of a single nanocrystal, Figure 2d, confirms the coexistence of Sn and S in individual particles. Therefore, optical, structural, and compositional analysis results are all consistent with the formation of quantum confined SnS nanocrystals, confirming that our single enzyme biomineralization approach can be extended for SnS biomineralization. As noted above, we have reported the application of our enzymatic direct biomineralization synthesis method to the formation of CuS and ZnS quantum confined nanocrystals,[34,35] and in combination, these results point to the feasibility of CZTS biomineralization.

Incubation of a buffered mixture of Cu acetate, Zn acetate, tin chloride (Cu:Zn:Sn = 1:2:2 molar ratios), L-cysteine, and smCSE for 6 h yields solutions and nanocrystals with significantly different optical properties to those where only one of the metal precursors is present, Figure 3a. The UV−vis absorption spectra, Figure 3a, and photoluminescence spectra, Figure S3, of CuS, SnS, and ZnS are consistent with the previously reported formation of quantum confined nanocrystals of these materials. In contrast, the UV−vis spectrum of CZTS shows broad absorption in the visible region with a shoulder at 375 nm, consistent with other reports for CZTS nanocrystals.[12,43] The corresponding photoluminescence of CZTS, Figure S3, shows a very low intensity, similar to the low intensity observed for Cu₂S, which is often attributed to partial oxidation of the CZTS particle.

The XRD pattern of the precipitated, centrifuged, and dried as-synthesized particles is consistent with the reported tetragonal structure of CZTS (space group *I-4*, ICDD 96-432-8659). The SEM-based XEDS spectrum for these particles confirms the coexistence of Cu, Zn, Sn, and S, Figure 3c, with an average composition of $Cu_{1.4}Zn_{1.3}Sn_{1.3}S_4$. Note that a variance between the relative ratios of the CZT cations in the synthesis solution and the final CZTS nanocrystals is frequently reported and is typically attributed to differences in reactivity of the precursors.[12,13,15,44,45] Also note that no chlorine signal is detected, as with the SnS particles in Figure 1.

As with SnS, direct evidence of CZTS alloy nanocrystal formation is provided by HAADF-STEM imaging, Figure 4a,b, FFT-based analysis of the structure of a single particle, Figure 4c and Table S2, and STEM−XEDS confirming the presence of Cu, Zn, Sn, and S in a single particle, Figure 4d.
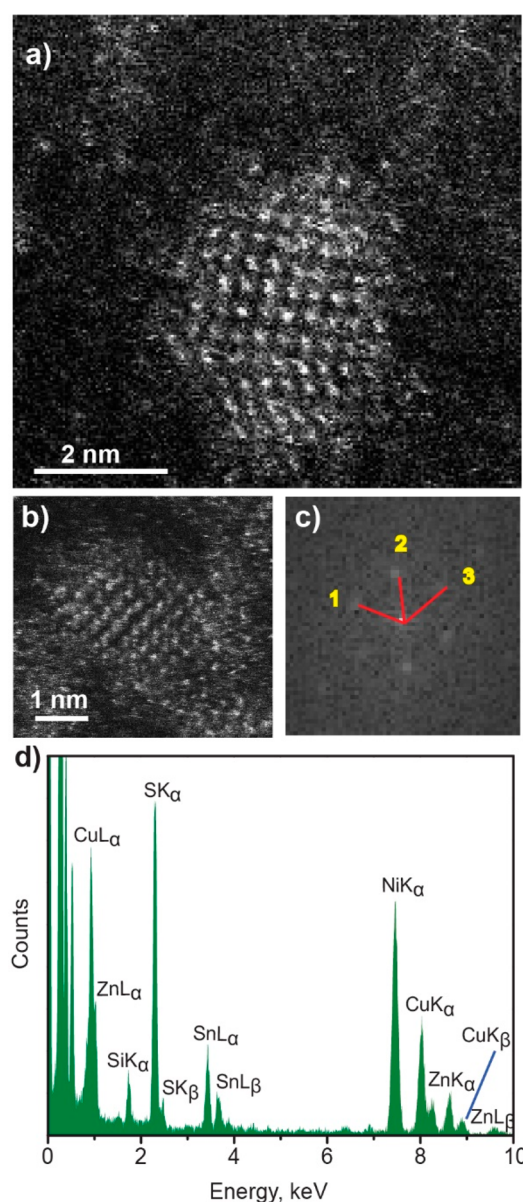
Figure 4. (a,b) Representative HAADF-STEM images, (c) FFT pattern corresponding to the image in b, and (d) STEM−XEDS spectrum of biomineralized CZTS showing the coexistence of Cu, Zn, Sn, and S in a cluster of particles with an average composition of $Cu_{1.4}Zn_{1.3}Sn_{1.3}S_4$. The Ni and Si peaks in this spectrum are artifacts and originate from the Ni-containing TEM grid and the Si-based XEDS detector, respectively.
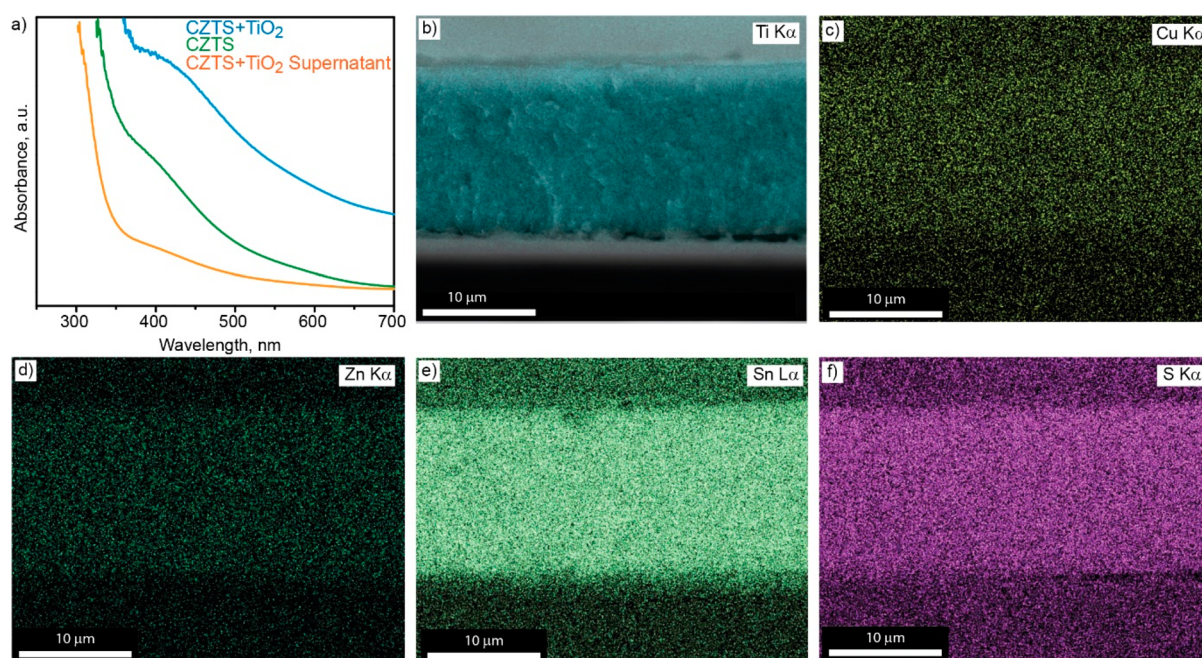
Figure 5. (a) UV−vis absorption spectrum of biomineralized CZTS after centrifugation (green line), the same particles after addition of TiO₂ particles (blue line), and the supernatant of the CZTS/TiO₂ mixture after centrifugation (orange line); (b) SEM cross-sectional view of the QDSSC TiO₂-based anode following in situ biomineralization of CZTS with superimposed XEDS map at the Ti Kα peak energy, corresponding XEDS maps at the (c) Cu Kα, (d) Zn Kα, (e) Sn Lα, and (f) S K$_\alpha$ peak energies.

The HAADF-STEM images show clear lattice fringes indicating crystalline material. Analysis of the corresponding FFT pattern indicates that the interplanar angles and spacings are consistent with reported values for tetragonal structured Cu₂ZnSnS₄ viewed along the [110] zone axis. Measurement of the diameters of more than 180 particles provides an average particle size of 3.85 ± 0.83 nm, Figure S4. The STEM−XEDS analysis on a single particle provides a composition of Cu₁.₄Zn₁.₃Sn₁.₃S₄. Optimization of the particle composition is discussed later in this manuscript.

3.2. Integration into Quantum Dot Sensitized Solar Cells. Obtaining a uniform distribution of well-anchored quantum dot sensitizers throughout the TiO₂ structure of the QDSSC electrode is thought to be critical for optimizing device performance. The attachment of our biomineralized CZTS to TiO₂ was first investigated by mixing TiO₂ particles into an as-synthesized nanocrystal solution. The UV−vis absorption spectrum of this CZTS/TiO₂ mixture shows strong absorption due to both TiO₂ and CZTS particles. Measuring the centrifuged supernatant of this mixture shows only background absorption, indicating that the CZTS nanocrystals adsorb onto the larger TiO₂ particles and are thus pelletized and removed from solution by centrifugation, Figure 5a. Note that as-synthesized CZTS particles are too small to be pelletized by the same centrifugation process in the absence of TiO₂. The UV−vis absorption spectra of as-synthesized CZTS in the absence of TiO₂ after centrifugation are the same as those of the original CZTS particles shown in Figure 3a. This confirms strong association between as-synthesized CZTS in the synthesis solution and the larger TiO₂ particles without requiring any further processing.

This spontaneous attachment of biomineralized CZTS nanocrystals enables the direct biomineralization of the nanocrystals within a preformed porous TiO₂ QDSSC electrode structure, in a process somewhat analogous to the use of chemical bath routes to grow QD sensitizers into TiO₂ by more traditional chemical syntheses. This in situ biomineralization was achieved by placing a presintered TiO₂ on an FTO electrode structure into the buffered biomineralization synthesis solution containing CSE enzyme, L-cysteine, and the Cu, Sn, and Zn precursors (Cu:Sn:Zn = 1:2:2 molar ratio). The electrode was then incubated in solution at 37 °C for 6 h, analogous to the CZTS particle synthesis method. SEM−XEDS maps across the resulting electrode show no discernible gradient in S Kα, Sn Lα,β, Cu Kα, or Zn Kα signals, Figure 5b−f. An individual SEM−XEDS spectrum taken from a spot within the TiO₂ layer is provided in Figure S5. This is indicative of an even distribution of the CZTS nanocrystals throughout the electrode being achieved by this in situ synthesis approach. Note that a small chlorine signal is detected in the QDSSC anode where it is absent in the pure particle spectra. This signal is likely due to some salt contamination.

In contrast, drop-casting of previously synthesized CZTS nanocrystals onto the surface of the TiO₂ electrode with subsequent drying leads to strong composition gradients and accumulation of sensitizer at the inactive TiO₂ surface rather than within the crucial TiO₂/FTO interface region. SEM−XEDS point analysis, Figure S6, at the TiO₂/FTO interface, center of the TiO₂ layer, and close to the TiO₂ surface, shows strong signals for Cu, Zn, Sn, and S at the surface but dramatically decreased intensity inside the anode and almost undetectable amounts near the interface, confirming this gradient in Cu₁.₄Zn₁.₃Sn₁.₃S₄ nanocrystal distribution.

This even distribution of the nanocrystals, stretching right up to the critical TiO₂/FTO interface region, achieved through in situ biomineralization, is reflected in substantially higher QDSSC J−V performance when compared with cells prepared by drop-casting of nominally identical nanocrystals onto the TiO₂ electrode surface. This latter approach gives a poorer distribution of the nanocrystals in the electrode. The J−V
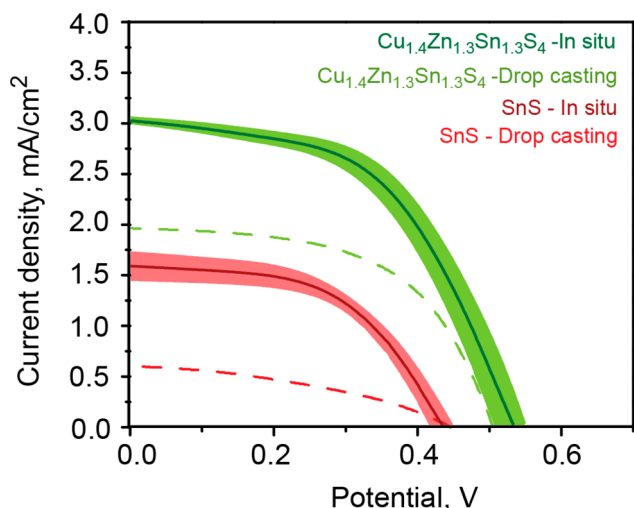
Figure 6. J−V curves of QDSSCs with TiO$_2$ anodes with drop-cast SnS (dashed red line), in situ biomineralized SnS (solid red line), drop-cast Cu$_{1.4}$Zn$_{1.3}$Sn$_{1.3}$S$_4$ (dashed green line), and in situ biomineralized Cu$_{1.4}$Zn$_{1.3}$Sn$_{1.3}$S$_4$ (solid red line) QDs. Shaded regions denote performance range of triplicate cells.

Figure 7. Ternary composition diagram of CZTS nanocrystals determined from SEM-EDAX analysis. The molar cation composition in the synthesis solution is indicated by open symbols, with the linked closed symbol denoting the composition of the synthesized nanocrystals.

performance curves and parameters for the resulting QDSSCs are provided in Figure 6 and Table S3.

For pure SnS nanocrystals, the performance improves from open circuit potential, V_{OC} = 0.45 V, short circuit current, J_{SC} = 0.60 mA/cm^2, and fill factor, FF = 39%, for drop-cast SnS to V_{OC} = 0.44 V, J_{SC} = 1.58 mA/cm^2, and FF = 53% for the in situ biomineralized SnS. The performance is further enhanced to V_{OC} = 0.51 V, J_{SC} = 1.96 mA/cm^2, and FF = 55%, by utilizing drop-cast Cu$_{1.4}$Zn$_{1.3}$Sn$_{1.3}$S$_4$ nanocrystals. The highest performance, V_{OC} = 0.53, J_{SC} = 3.10 mA/cm^2, and FF = 62%, was achieved through in situ synthesis of Cu$_{1.4}$Zn$_{1.3}$Sn$_{1.3}$S$_4$ nanocrystals, Figure 6. The similarity in V_{OC} between drop-cast and in situ formed cells for each composition is expected, as the particle synthesis process is nominally identical in both the presynthesized and in situ synthesized photoanodes, such that size, composition, and resulting optical band gap should be nominally identical. The improvement in short circuit current is directly attributable to the increased concentration of CZTS nanocrystals within the critical interfacial region of the cathode. Any possible detrimental impact of residual enzyme on cell performance is overcome by the improvement in nanocrystal distribution but remains a topic for future study.

Note that data for two control experiments, Figure S7 and Table S3, utilizing just (i) a pure TiO$_2$ electrode structure and (ii) a TiO$_2$ electrode incubated in the biomineralization solution in the absence of metal cations show substantially lower current densities and V_{oc} values. This second control experiment confirms no significant role of the enzyme or generated reactive sulfur. The small performance improvement observed is likely due to some sulfur deposition on the surface of the TiO$_2$.

3.3. Particle Composition Control. As noted earlier, the highest performing CZTS composition is reported to lie closer to the stoichiometric Cu$_2$SnZnS$_4$ composition rather than the Cu$_{1.4}$Zn$_{1.3}$Sn$_{1.3}$S$_4$ material produced from the stoichiometric 2:1:1 mixture of cation salts in the synthesis solution.[12,13,15,44,45] We thus investigated manipulating the metal cation ratios in the biomineralization synthesis solution as a route to control CZTS nanocrystal composition. The resulting nanocrystal composition, determined from SEM−XEDS analysis, as a function of cation
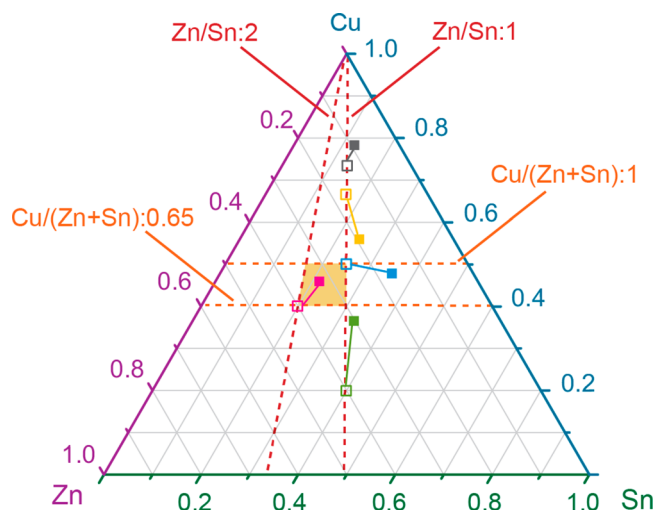
ratio in solution, is plotted on a ternary diagram in Figure 7, and further details are provided in Table S4. The suggested composition region for the highest QDSSC performance is highlighted in Figure 7. The nanocrystal composition we achieved that was closest to the suggested optimal Cu$_2$ZnSnS$_4$ was Cu$_{1.9}$Zn$_{1.2}$Sn$_{0.9}$S$_4$, which was synthesized from a solution with an initial 2:2:1 atomic ratio of Cu:Zn:Sn. We note that while the resulting particle composition is reflective of the relative ratios of metal ions in the precursor solution, as with chemical synthesis routes, the composition of the particles is not the same as that in solution and is, in general, enriched in Cu.

This difference between solution and particle composition has been widely reported[12,13,15,44,45] and agrees in this case with the previous report by Shavel et al. for organic-phase synthesis of Cu$_2$SnSnS$_4$, where an increased Cu ratio is attributed to the more rapid reaction of the Cu precursor with sulfur.[44] Based on such considerations, Chesman et al. utilized a similar approach of reducing the Cu concentration in the precursor solution to tune the composition of the final nanocrystal to be closer to the desired ratio.[45] While our synthesis occurs in the aqueous phase, we may anticipate a similar explanation. We have previously reported that the nanocrystal biomineralization mechanism relies on the reaction between a chelated metal precursor and dissolved HS$^-$ formed by the enzyme in solution.[36] The biomineralization solution contains an excess of L-cysteine in relation to the metal cations, such that we would expect the metal cations to be fully chelated by L-cysteine with Cu(II) reported to have a higher binding affinity to L-cysteine in aqueous solution than Zn(II).[46] We have previously noted significant differences in metal sulfide nanoparticle formation rate as we change the metal precursor, for example, conducting PbS synthesis at 4 °C in order to reduce the rate to prevent rapid precipitation of bulk material.[33] As such, the variations in composition are most likely due to differences in precursor reaction rates.

Detailed microstructural analysis was conducted to confirm the crystallinity and composition of the optimized Cu$_{1.9}$Zn$_{1.2}$Sn$_{0.9}$S$_4$ particles. A representative HAADF-STEM image of these CZTS particles is shown in Figure 8a. A particle size distribution was derived from analysis of 169 particles, Figure S8, demonstrating a
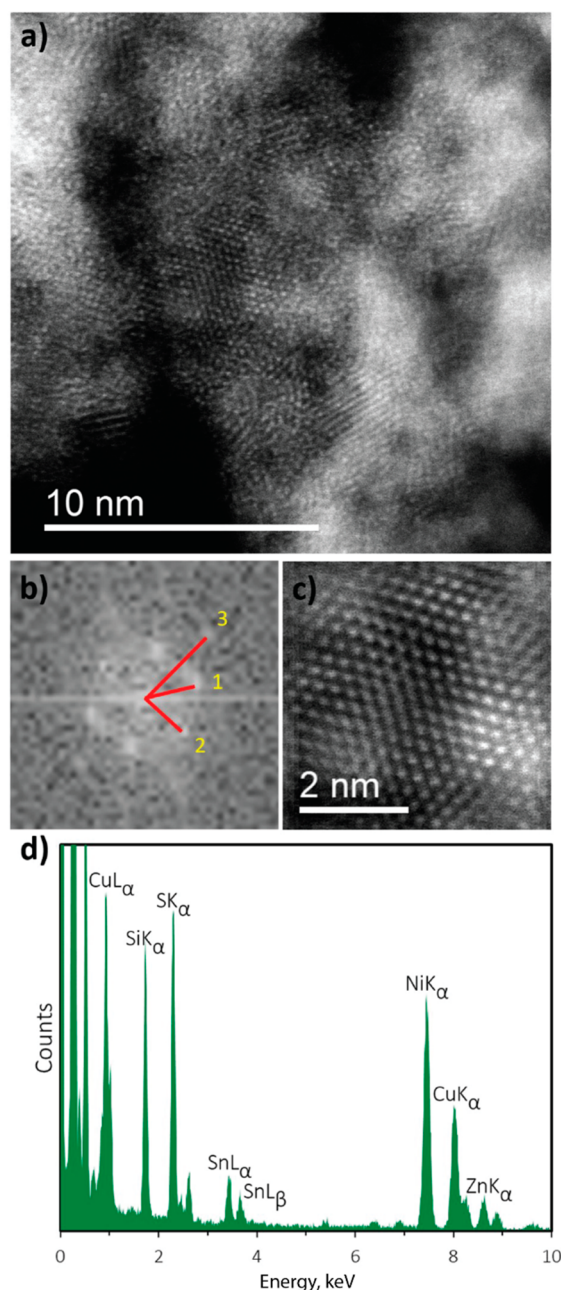
Figure 8. (a) Representative HAADF-STEM image; (b) FFT pattern corresponding to the image in c; (c) a filtered region of interest from image a; and (d) an XEDS spectrum from 10 particles showing a mean composition of $Cu_{2.4}Zn_{0.75}Sn_{0.95}S_4$. Ni and Si peaks are present as artifacts from the Ni grid and Si detector.

mean diameter of 2.96 ± 0.69 nm. Figure 8b is an FFT pattern obtained from the area shown as a filtered image in Figure 8c. Analysis of the interplanar spacings and angles, Table S5, in this image shows it to be consistent with the $[\bar{2}01]$ zone axis of $Cu_{1.9}Zn_{1.2}Sn_{0.9}S_4$. Quantitative analysis of the STEM–XEDS data collected from a region containing 10 particles gives an average composition of $Cu_{2.3}Zn_{0.75}Sn_{0.95}S_4$ or a ratio of copper to zinc to tin of 2.4:0.8:1. While this differs from the SEM-based XEDS composition shown in Figure 7, when considering the errors that are associated in both cases with the use of precalculated coefficients for quantitative analysis, this measurement is within a 95% confidence interval of the composition of SEM-based $Cu_{1.9}Zn_{1.2}Sn_{0.9}S_4$ or a ratio of Cu to Zn to Sn of 2.1:1.3:1.
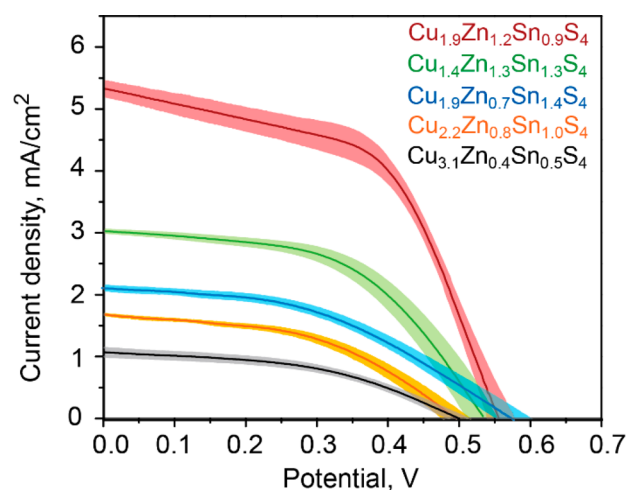
Figure 9. QDSSC $J-V$ curves for cells with TiO_2 anodes and incorporating in situ biomineralized CZTS with denoted composition. The shaded regions represent the performance ranges measured for triplicate cells.

Finally, these optimized particles and related compositions from Figure 7 were incorporated by in situ biomineralization within QDSSC electrodes, Figure 9 and Table S5. As may be anticipated, the closer the composition is to the suggested ideal compositional region highlighted in Figure 7, the higher the solar cell performance, with the $Cu_{1.9}Zn_{1.2}Sn_{0.9}S_4$ CZTS nanocrystals providing the highest performance, $V_{OC} = 0.55$ V, $J_{SC} = 5.35$ mA/cm^2, and FF = 65%, when directly biomineralized within the TiO_2 layer. Performance metrics for all solar cells that were manufactured are provided in Table S6. While the cell performance is not fully optimized, these performance trends support the efficacy of controlled composition ternary alloy quantum dot biomineralization and the feasibility of integrating these materials into devices.

4. CONCLUSIONS

Single enzyme direct biomineralization is an ambient temperature, facile approach to the synthesis of CZTS nanocrystals. The Cu, Zn, and Sn ratios in the final nanocrystals can be tuned through the composition of the biomineralization solution; however, the correlation is not direct. In general, the nanoparticles are Cu deficient compared to the synthesis solution, most likely due to differences in reactivity between the cations in solution and the HS^- generated in solution via the enzymatic turnover of L-cysteine. This biomineralization process can be conducted directly within a preformed TiO_2 QDSSC anode structure to achieve an even distribution of sensitizers throughout the electrode. Such an even distribution enhances the cell performance further when compared to simple drop-casting of preformed CZTS quantum dots onto the electrode surface.

■ ASSOCIATED CONTENT

Ⓢ Supporting Information

The Supporting Information is available free of charge at https://pubs.acs.org/doi/10.1021/acsami.9b15545.

Additional structural and optical characterization of the SnS and CZTS nanocrystals including particle size distributions, lattice fitting, and photoluminescence spectra. Supplementary characterization of the solar cells includes SEM–XEDS data of the drop-cast cell anode, tabulated performance parameters, blank cell performance, and

SEM−XEDS composition data for the CZTS composition optimization study (PDF)

■ AUTHOR INFORMATION

Corresponding Author

*E-mail: mcintosh@lehigh.edu.

ORCID

Li Lu: 0000-0002-6688-1176

Steven McIntosh: 0000-0003-4664-2028

Notes

The authors declare no competing financial interest.

■ ACKNOWLEDGMENTS

■ REFERENCES

(1) Li, T.; Lee, Y.; Teng, H. High-performance quantum dot-sensitized solar cells based on sensitization with CuInS2 quantum dots/CdS heterostructure. *Energy Environ. Sci.* **2012**, *5*, 5315−5324.

(2) Im, S. H.; Kim, H.; Kim, S. W.; Kim, S.; Seok, S. I. All solid state multiply layered PbS colloidal quantum-dot-sensitized photovoltaic cells. *Energy Environ. Sci.* **2011**, *4*, 4181−4186.

(3) Chebrolu, V. T.; Kim, H. Recent progress in quantum dot sensitized solar cells: an inclusive review of photoanode, sensitizer, electrolyte, and the counter electrode. *J. Mater. Chem. C* **2019**, *7*, 4911−4933.

(4) Zhou, H.; Hsu, W.; Duan, H.; Bob, B.; Yang, W.; Song, T.; Hsu, C.; Yang, Y. CZTS nanocrystals: a promising approach for next generation thin film photovoltaics. *Energy Environ. Sci.* **2013**, *6*, 2822−2838.

(5) Katagiri, H.; Jimbo, K.; Maw, W. S.; Oishi, K.; Yamazaki, M.; Araki, H.; Takeuchi, A. Development of CZTS-based thin film solar cells. *Thin Solid Films* **2009**, *517*, 2455−2460.

(6) Guo, Q.; Hillhouse, H. W.; Agrawal, R. Synthesis of Cu2ZnSnS4 Nanocrystal Ink and Its Use for Solar Cells. *J. Am. Chem. Soc.* **2009**, *131*, 11672−11673.

(7) Suryawanshi, M. P.; Agawane, G. L.; Bhosale, S. M.; Shin, S. W.; Patil, P. S.; Kim, J. H.; Moholkar, A. V. CZTS based thin film solar cells: a status review. *Mater. Technol.* **2013**, *28*, 98−109.

(8) Wang, Z.; Demopoulos, G. P. Growth of Cu_2ZnSnS_4 Nanocrystallites on TiO_2 Nanorod Arrays as Novel Extremely Thin Absorber Solar Cell Structure via the Successive-Ion-Layer-Adsorption-Reaction Method. *ACS Appl. Mater. Interfaces* **2015**, *7*, 22888−22897.

(9) Tang, R.; Xie, Z.; Zhou, S.; Zhang, Y.; Yuan, Z.; Zhang, L.; Yin, L. Cu2ZnSnS4 Nanoparticle Sensitized Metal–Organic Framework Derived Mesoporous TiO2 as Photoanodes for High-Performance Dye-Sensitized Solar Cells. *ACS Appl. Mater. Interfaces* **2016**, *8*, 22201−22212.

(10) Dai, P.; Zhang, G.; Chen, Y.; Jiang, H.; Feng, Z.; Lin, Z.; Zhan, J. Porous copper zinc tin sulfide thin film as photocathode for double junction photoelectrochemical solar cells. *Chem. Commun.* **2012**, *48*, 3006−3008.

(11) Wang, Y.; Li, C.; Yin, X.; Wang, H.; Gong, H. Cu2ZnSnS4 (CZTS) Application in TiO2 Solar Cell as Dye. *ECS J. Solid State Sci. Technol.* **2013**, *2*, Q95−Q98.

(12) Cao, M.; Shen, Y. A mild solvothermal route to kesterite quaternary Cu2ZnSnS4 nanoparticles. *J. Cryst. Growth* **2011**, *318*, 1117−1120.

(13) Xie, W.; Jiang, X.; Zou, C.; Li, D.; Zhang, J.; Quan, J.; Shao, L. Synthesis of highly dispersed Cu2ZnSnS4 nanoparticles by solvothermal method for photovoltaic application. *Phys. E* **2012**, *45*, 16−20.

(14) Riha, S. C.; Parkinson, B. A.; Prieto, A. L. Solution-Based Synthesis and Characterization of Cu2ZnSnS4 Nanocrystals. *J. Am. Chem. Soc.* **2009**, *131*, 12054−12055.

(15) Shin, S. W.; Han, J. H.; Park, C. Y.; Moholkar, A. V.; Lee, J. Y.; Kim, J. H. Quaternary Cu2ZnSnS4 nanocrystals: Facile and low cost synthesis by microwave-assisted solution method. *J. Alloys Compd.* **2012**, *516*, 96−101.

(16) Steinhagen, C.; Panthani, M. G.; Akhavan, V.; Goodfellow, B.; Koo, B.; Korgel, B. A. Synthesis of Cu2ZnSnS4 nanocrystals for use in low-cost photovoltaics. *J. Am. Chem. Soc.* **2009**, *131*, 12554−12555.

(17) Cao, Y.; Denny, M. S.; Caspar, J. V.; Farneth, W. E.; Guo, Q.; Ionkin, A. S.; Johnson, L. K.; Lu, M.; Malajovich, I.; Radu, D.; Rosenfeld, H. D.; Choudhury, K. R.; Wu, W. High-Efficiency Solution-Processed Cu2ZnSn(S,Se)4 Thin-Film Solar Cells Prepared from Binary and Ternary Nanoparticles. *J. Am. Chem. Soc.* **2012**, *134*, 15644−15647.

(18) Katagiri, H.; Jimbo, K.; Tahara, M.; Araki, H.; Oishi, K. The Influence of the Composition Ratio on CZTS-based Thin Film Solar Cells. *MRS Proceedings* **2009**, *1165*, 1165-M04-01.

(19) Aldakov, D.; Lefrançois, A.; Reiss, P. Ternary and quaternary metal chalcogenide nanocrystals: synthesis, properties and applications. *J. Mater. Chem. C* **2013**, *1*, 3756−3776.

(20) Mitzi, D. B.; Gunawan, O.; Todorov, T. K.; Wang, K.; Guha, S. The Path Towards a High-Performance Solution-Processed Kesterite Solar Cell. *Sol. Energy Mater. Sol. Cells* **2011**, *95*, 1421−1436.

(21) Todorov, T. K.; Reuter, K. B.; Mitzi, D. B. High-Efficiency Solar Cell with Earth-Abundant Liquid-Processed Absorber. *Adv. Mater.* **2010**, *22*, E156−E159.

(22) Agawane, G. L.; Kamble, A. S.; Vanalakar, S. A.; Shin, S. W.; Gang, M. G.; Yun, J. H.; Gwak, J.; Moholkar, A. V.; Kim, J. H. Fabrication of 3.01% Power Conversion Efficient High-Quality CZTS Thin Film Solar Cells by a Green and Simple Sol−gel Technique. *Mater. Lett.* **2015**, *158*, 58−61.

(23) Suryawanshi, M. P.; Shin, S. W.; Ghorpade, U. V.; Gurav, K. V.; Hong, C. W.; Agawane, G. L.; Vanalakar, S. A.; Moon, J. H.; Yun, J. H.; Patil, P. S.; Kim, J. H.; Moholkar, A. V. Improved Photoelectrochemical Performance of Cu2ZnSnS4 (CZTS) Thin Films Prepared using Modified Successive Ionic Layer Adsorption and Reaction (SILAR) Sequence. *Electrochim. Acta* **2014**, *150*, 136−145.

(24) Mali, S. S.; Patil, B. M.; Betty, C. A.; Bhosale, P. N.; Oh, Y. W.; Jadkar, S. R.; Devan, R. S.; Ma, Y.; Patil, P. S. Novel synthesis of kesterite Cu2ZnSnS4 nanoflakes by successive ionic layer adsorption and reaction technique: characterization and application. *Electrochim. Acta* **2012**, *66*, 216−221.

(25) Shinde, N.; Dubal, D.; Dhawale, D.; Lokhande, C.; Kim, J.; Moon, J. Room temperature novel chemical synthesis of Cu2ZnSnS4 (CZTS) absorbing layer for photovoltaic application. *Mater. Res. Bull.* **2012**, *47*, 302−307.

(26) Henry, J.; Mohanraj, K.; Sivakumar, G. Electrical and optical properties of CZTS thin films prepared by SILAR method. *Journal of Asian Ceramic Societies* **2016**, *4*, 81−84.

(27) Shin, B.; Gunawan, O.; Zhu, Y.; Bojarczuk, N. A.; Chey, S. J.; Guha, S. Thin film solar cell with 8.4% power conversion efficiency using an earth-abundant Cu2ZnSnS4 absorber. *Prog. Photovoltaics* **2013**, *21*, 72−76.

(28) Woo, K.; Kim, Y.; Moon, J. A non-toxic, solution-processed, earth abundant absorbing layer for thin-film solar cells. *Energy Environ. Sci.* **2012**, *5*, 5340−5345.

(29) Yang, Z.; Lu, L.; Berard, V. F.; He, Q.; Kiely, C. J.; Berger, B. W.; McIntosh, S. Biomanufacturing of CdS quantum dots. *Green Chem.* **2015**, *17*, 3775−3782.

(30) Dunleavy, R.; Lu, L.; Kiely, C. J.; McIntosh, S.; Berger, B. W. Single-enzyme biomineralization of cadmium sulfide nanocrystals with controlled optical properties. *Proc. Natl. Acad. Sci. U. S. A.* **2016**, *113*, 5275.

(31) Jun, H. K.; Careem, M. A.; Arof, A. K. Quantum dot-sensitized solar cells—perspective and recent developments: A review of Cd chalcogenide quantum dots as sensitizers. *Renewable Sustainable Energy Rev.* **2013**, *22*, 148−167.

(32) Kouhnavard, M.; Ikeda, S.; Ludin, N. A.; Ahmad Khairudin, N. B.; Ghaffari, B. V.; Mat-Teridi, M. A.; Ibrahim, M. A.; Sepeai, S.; Sopian, K. A review of semiconductor materials as sensitizers for quantum dot-sensitized solar cells. *Renewable Sustainable Energy Rev.* **2014**, *37*, 397−407.

(33) Spangler, L. C.; Lu, L.; Kiely, C. J.; Berger, B. W.; McIntosh, S. Biomineralization of PbS and PbS@CdS core@shell nanocrystals and their application in quantum dot sensitized solar cells. *J. Mater. Chem. A* **2016**, *4*, 6107−6115.

(34) Sadeghnejad, A.; Lu, L.; Kiely, C. J.; Berger, B. W.; McIntosh, S. Single enzyme direct biomineralization of ZnS, $Zn_xCd_{1-x}S$ and $Zn_xCd_{1-x}S$@ZnS quantum confined nanocrystals. *RSC Adv.* **2017**, *7*, 38490−38497.

(35) Spangler, L. C.; Chu, R.; Lu, L.; Kiely, C. J.; Berger, B. W.; McIntosh, S. Enzymatic biomineralization of biocompatible CuInS2, (CuInZn)S2 and CuInS2/ZnS core/shell nanocrystals for bioimaging. *Nanoscale* **2017**, *9*, 9340−9351.

(36) Spangler, L. C.; Cline, J. P.; Kiely, C. J.; McIntosh, S. Low temperature aqueous synthesis of size-controlled nanocrystals through size focusing: a quantum dot biomineralization case study. *Nanoscale* **2018**, *10*, 20785−20795.

(37) Kumnorkaew, P.; Ee, Y.; Tansu, N.; Gilchrist, J. F. Investigation of the Deposition of Microsphere Monolayers for Fabrication of Microlens Arrays. *Langmuir* **2008**, *24*, 12150−12157.

(38) Zhao, K.; Yu, H.; Zhang, H.; Zhong, X. Electroplating cuprous sulfide counter electrode for high-efficiency long-term stability quantum dot sensitized solar cells. *J. Phys. Chem. C* **2014**, *118*, 5683−5690.

(39) Ning, J.; Men, K.; Xiao, G.; Wang, L.; Dai, Q.; Zou, B.; Liu, B.; Zou, G. Facile synthesis of IV-VI SnS nanocrystals with shape and size control: Nanoparticles, nanoflowers and amorphous nanosheets. *Nanoscale* **2010**, *2*, 1699−1703.

(40) Johnson, J. B.; Jones, H.; Latham, B. S.; Parker, J. D.; Engelken, R. D.; Barber, C. Optimization of photoconductivity in vacuum-evaporated tin sulfide thin films. *Semicond. Sci. Technol.* **1999**, *14*, 501−507.

(41) Tripathi, A. M.; Mitra, S. Tin sulfide (SnS) nanorods: structural, optical and lithium storage property study. *RSC Adv.* **2014**, *4*, 10358−10366.

(42) Deepa, K. G.; Nagaraju, J. Development of SnS quantum dot solar cells by SILAR method. *Mater. Sci. Semicond. Process.* **2014**, *27*, 649−653.

(43) Zhou, Y.; Zhou, W.; Du, Y.; Li, M.; Wu, S. Sphere-like kesterite Cu_2ZnSnS_4 nanoparticles synthesized by a facile solvothermal method. *Mater. Lett.* **2011**, *65*, 1535−1537.

(44) Shavel, A.; Cadavid, D.; Ibanez, M.; Carrete, A.; Cabot, A. Continuous Production of Cu2ZnSnS4 Nanocrystals in a Flow Reactor. *J. Am. Chem. Soc.* **2012**, *134*, 1438−1441.

(45) Chesman, A. S. R.; van Embden, J.; Duffy, N. W.; Webster, N. A. S.; Jasieniak, J. J. In Situ Formation of Reactive Sulfide Precursors in the One-Pot, Multigram Synthesis of Cu2ZnSnS4 Nanocrystals. *Cryst. Growth Des.* **2013**, *13*, 1712−1720.

(46) Lenz, G. R.; Martell, A. E. Metal Chelates of Some Sulfur-containing Amino Acids*. *Biochemistry* **1964**, *3*, 745−750.